Dynamics of transverse waves and zigzag instabilities in photorefractive two-wave mixing with a feedback mirror

O. Sandfuchs and F. Kaiser

Institute of Applied Physics, Darmstadt University of Technology, Hochschulstrasse 4a, 64289 Darmstadt, Germany

M. R. Belić

Institute of Physics, P.O. Box 57, 11001 Belgrade, Yugoslavia

Received May 30, 2000; revised manuscript received October 27, 2000

We report on the appearance of running transverse waves and zigzag instabilities in photorefractive counterpropagating two-wave mixing with a single external feedback mirror. These secondary structures are caused by the sluggish temporal response of the crystal through the buildup of a reflection grating. We derive a Landau-type equation for the critical mode amplitude above the primary instability threshold and compare it with the results from numerical simulations in the case of low and high optical aspect ratios. The effect of intensity-dependent relaxation time on the formation of the spatiotemporal structures is discussed. © 2001 Optical Society of America

OCIS codes: 190.4420, 190.5330, 190.7070.

1. INTRODUCTION

Since the initial experimental observations of hexagonal patterns[1,2] that result from counterpropagation of two optical beams in photorefractive (PR) crystals, pattern formation through PR two-wave mixing has become a growing field of nonlinear optics. Owing to potential applications for parallel optical data and image processing by PR devices, much research effort has been invested in the examination of the nature of transverse spatiotemporal structures in these systems.

In particular, the formation of patterns in counterpropagating two-wave mixing with a feedback mirror has been the topic of a number of papers that have appeared recently. They were mostly experimental studies in which the spontaneous formation of hexagons was observed.[3–5] Although hexagons were the predominantly observed structure, other structures, such as stripes and squares, have also been identified.[6] Theoretical investigations have been few. They treated the onset of transverse structures by means of linear stability analyses[7,8] and described the stabilization of hexagonal mode structures by using an amplitude equation formalism.[9] The difficulties in analytical or numerical treatment of the two-wave mixing equations in reflection geometry arise both from the nonlocal PR medium response, which results in an energy transfer between the beams, and from the fact that the photorefractive relaxation time is intensity dependent.

In general, diffraction and nonlinear beam coupling lead to the formation of transverse patterns. Optical beams and the refractive-index grating that couples the beams become spontaneously unstable against transverse modulations. These patterns grow as an absolute instability out of the initially smooth beam and grating profiles. The model for the PR grating response originates from a charge-transport model formulated by Kukhtarev *et al.*[10] Rigorous solutions of Kukhtarev's nonlinear material equations are computationally expensive.[11] In the context of pattern formation through the interaction of counterpropagating waves via reflection gratings, it is particularly desirable to have an approximation of the grating response that is as simple as possible but is still good enough to account for most of the phenomena observed. Otherwise this problem will quickly become unwieldy and render analytical and even numerical treatment extremely difficult, even in the limit of one transverse dimension.

A model of wave mixing that possesses such qualities is introduced in Section 2. In addition to providing an appropriate description of the pseudoequilibrium grating response below the dynamic instability threshold,[12] this model is capable of elucidating the temporal evolution of the medium response and has proved useful in applications to spatiotemporal pattern formation through two-wave mixing and four-wave mixing in PR media.[13–16] In Section 3 of the paper we deal with the linear and nonlinear behavior of transverse patterns, and Section 4 brings conclusions.

Although it may be imperative to move to two transverse dimensions in numerical simulations to be able properly to view the formation of patterns, massive computational needs for high resolution in three spatial dimensions and prolonged observation in time make such a move numerically expensive. Because of the analogies between one-dimensional modulation and two-dimensional stripe patterns we are convinced that the one-dimensional study still reveals important features of the appearance and the dynamics of transverse patterns.

0740-3224/2001/040505-10$15.00

With one spatial dimension fewer to worry about, one can apply the full numerical power to understand better the onset of primary and secondary instabilities and their long-time behavior. In such a frame of mind, we set out to investigate analytically and numerically the formation of patterns and the effects of intensity-dependent relaxation time on these patterns in the photorefractive feedback system.

2. THEORETICAL MODEL

The geometry of the standard setup for observation of transverse patterns in two-wave mixing with reflection gratings and one feedback mirror is presented in Fig. 1. The wave-mixing process is described by the slowly varying envelope paraxial equations for the two beams:

$$\partial_z A_1 + if\partial_x^2 A_1 = -QA_2, \tag{1a}$$

$$-\partial_z A_2 + if\partial_x^2 A_2 = Q^* A_1, \tag{1b}$$

where z is the propagation coordinate scaled by crystal length L; f is proportional to the inverse of the Fresnel number, $f = (4\pi F)^{-1} = L/(2k_0 w_0^2)$, where k_0 denotes the wave vector within the crystal in the propagation direction; and x is scaled by beam waist w_0. Q is the amplitude of the reflection grating, whose temporal evolution is described by a relaxation equation of the form

$$\tau(I)\partial_t Q + Q = \Gamma \frac{A_1 A_2^*}{I}, \tag{2}$$

where Γ is the wave-coupling constant. In PR wave mixing, $\tau(I) = (I_p/I)^\kappa \tau_{\mathrm{PR}}$ is, in general, the intensity-dependent relaxation time of the crystal, with total intensity $I = |A_1|^2 + |A_2|^2 + I_d$. Exponent κ describes the characteristic behavior of the nonlinear charge diffusion processes that are present in PR materials (see also Subsection 3.B below). Dark intensity I_d, because of thermal background illumination, is considered small ($I_d \sim 10^{-5} I_p$) compared with input pump beam $I_p = |A_1(z = 0, x = 0)|^2$. As τ_{PR} is a constant that depends only on material properties, it defines a natural scaling of time. The assumptions for Eqs. (1) and (2) are that the dynamics of envelopes is slaved to the grating amplitude, because of its slow evolution, and that the spatial distribution of Q is determined by the spatial distribution of the beam envelopes.

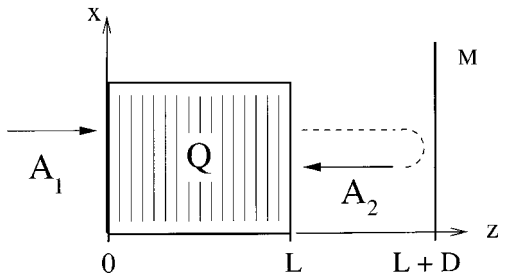

Fig. 1. Two-wave mixing configuration in reflection geometry: M, feedback mirror; A_1, pump beam; A_2, reflected beam; Q, grating amplitude; z, direction of propagation; x, transverse dimension; L, crystal length; D, distance to the feedback mirror.

3. LINEAR AND NONLINEAR BEHAVIOR OF TRANSVERSE STRUCTURES

Our investigation proceeds along two tracks, analytical and numerical. Analytically, we perform a linear stability analysis of Eqs. (1) and (2), along the lines introduced in Ref. 16. We do not restrict ourselves to stationary instabilities but allow for temporal variation and determine the primary instability threshold. Coupling constant Γ acts as the bifurcation parameter. To describe pattern formation beyond the primary threshold analytically, we obtain a Landau-type equation for the critical mode amplitude by performing a multiple scale expansion of Eqs. (1) and (2). Therefore we consider the time and space evolution of deviations $a_{1,2}$ and q from the fixed-point plane-wave solutions:

$$A_{1;2}(x, z, t) = A_{1;2}^0(z)[1 + a_{1;2}(x, z, t)], \tag{3a}$$

$$Q(x, z, t) = Q^0(z)[1 + q(x, z, t)]. \tag{3b}$$

On substituting into Eqs. (1) and (2), one obtains an equivalent set of nonlinear wave-mixing equations for the deviations, which reads as

$$\partial_z a_1 + if\partial_x^2 a_1 = \Gamma \frac{1}{1 + r^0}(a_1 - a_2 - q - a_2 q), \tag{4a}$$

$$-\partial_z a_2 + if\partial_x^2 a_2 = \Gamma \frac{r^0}{1 + r^0}(a_1 - a_2 + q^* + a_1 q^*), \tag{4b}$$

$$\left(\frac{1 + r^0}{N}\right)^\kappa \tau(I^0)\partial_t q + q = \frac{(a_1 - a_2)(1 + a_2^*) - r^0(a_1^* - a_2^*)(1 + a_1)}{r^0(1 + a_1)(1 + a_1^*) + (1 + a_2)(1 + a_2^*)}, \tag{4c}$$

where $I^0(z) = |A_1^0(z)|^2 + |A_2^0(z)|^2$ is the total plane-wave intensity and $r^0(z) = |A_1^0(z)|^2/|A_2^0(z)|^2$ is the ratio of plane-wave intensities, both of which, in general, depend on longitudinal position z. Denominator N is identical to the denominator of the right-hand side of Eq. (4c). Equations (4) are supplemented with the following boundary conditions:

$$a_1(x, 0, t) \equiv 0 \tag{5a}$$

$$a_2(x, L, t) = \sqrt{R}(\mathrm{FT})^{-1}\{\exp(i\phi)\mathrm{FT}[a_1(x, L, t)]\}. \tag{5b}$$

The quantity $\phi = 2fK^2 D/(n_0 L)$ is the propagation phase, D is the distance to the feedback mirror, and K is the wave vector of the spatial Fourier modes (FT denotes a Fourier transform). R is the mirror reflectivity, and n_0 is the crystal's homogeneous refractive index.

For the general procedure of multiple scale analysis in a bulk medium, for which we follow an idea of Geddes *et al.*,[17] it is convenient to choose a real basis for the state vectors of deviations by using the following transformation (see Appendix A): $(a_1, a_1^*, a_2, a_2^*)^T \rightarrow \mathbf{U} = (U_1, U_2, U_3, U_4)^T$ and $(q, q^*)^T \rightarrow \mathbf{P} = (P_1, P_2)^T$, which brings Eqs. (4) into the general form

$$\mathcal{L}_{z,x}\mathbf{U} + \mathcal{M}_0\mathbf{P} = \boldsymbol{\mathcal{M}}_1(\mathbf{P}|\mathbf{U}), \tag{6a}$$

$$(\mathcal{D}_{0,t} + \mathcal{D}_{1,t}(\mathbf{U}) + \mathcal{D}_{2,t}(\mathbf{U}|\mathbf{U}) + \ldots)\mathbf{P} - \mathcal{N}_0\mathbf{U} = \boldsymbol{\mathcal{N}}_1(\mathbf{U}|\mathbf{U}) + \boldsymbol{\mathcal{N}}_2(\mathbf{U}|\mathbf{U}|\mathbf{U}) + \ldots . \tag{6b}$$

Here the matrices $\mathcal{L}_{z,x}$ and $\mathcal{D}_{j,t}$ are the spatial and temporal derivative operators, respectively, $\mathcal{M}_0$ and $\mathcal{N}_0$ are composed of the coefficients of the linear coupling between the field and the grating, and $\boldsymbol{\mathcal{M}}_j$ and $\boldsymbol{\mathcal{N}}_j$ are vectors that describe nonlinear field–grating and field–field interactions, respectively. Owing to the intensity dependence of the PR relaxation time, the temporal evolution contributes to linear $\mathcal{D}_{0,t}$ and nonlinear $\mathcal{D}_{j,t}$ terms ($j = 1,2,\ldots$).

The multiple scale analysis for obtaining a Landau-type equation is based on the fact that in the neighborhood of bifurcation point Γ_c the temporal evolution is separable into fast and slow scales. For details of the multiple scale expansion see Appendix A. The solution ansatz in the 1st order introduces amplitude W of critical mode K_c. Expanding Eqs. (6) to 3rd order of nonlinearity results in resonant mode interaction in the amplitude equation of the critical mode [see Eq. (A21) below]:

$$\tau_0 d_t W = (\Gamma - \Gamma_c)W - g_s|W|^2W. \tag{7}$$

This is the well-known Landau equation. It provides a universal description of the self-organization of patterns in one dimension,[18] in which case the beam modulation corresponds to a stripe pattern in two dimensions. The critical mode amplitude acts as the order parameter. The relaxation rate

$$\tau_0 = \frac{1}{g_0}\langle \mathbf{v}_{K_c}|\mathcal{M}_0^c\tau(I^0)\mathcal{N}_0|\mathbf{u}_{K_c}^{(1)}\rangle, \tag{8}$$

which is a function of κ through $\tau(I^0) = [I_p/I^0(z)]^\kappa\tau_{\mathrm{PR}}$, and the nonlinear self-coupling coefficient

$$g_s = \frac{1}{g_0}\langle \mathbf{v}_{K_c}|\mathbf{m}_s - \mathcal{M}_0^c\mathbf{n}_s\rangle, \tag{9}$$

together with $g_0 = \langle \mathbf{v}_{K_c}|\tilde{\mathcal{M}}_0\mathcal{N}_0 - \tilde{\mathcal{L}}|\mathbf{u}_{K_c}^{(1)}\rangle$, are defined through scalar products that involve integrals over dz and contain the linear eigenfunction $\mathbf{u}_{K_c}^{(1)}(z)$ of the critical mode and those of modes $K = 0$ and $K = 2K_c$ [which appear in the 2nd order through $\mathbf{m}_s(z)$ and $\mathbf{n}_s(z)$; Eqs. (A22) and (A23) below] multiplied by linear adjoint eigenfunction $\mathbf{v}_{K_c}(z)$. The coefficients reflect the specific characteristics of the photorefractive system under consideration, and their numerical values are given in the following subsections.

To corroborate our analytical results near the primary threshold, and to investigate the system behavior far above it, we performed numerical simulations of the fully nonlinear system, using a split-step beam propagation method developed earlier[16] and appropriately modified to account for the feedback mirror.

In optics, unlike in most of the hydrodynamic systems, e.g., the beam profiles are constrained to a finite lateral extent. A laser beam has typically a Gaussian envelope, and the aspect ratio is low. A higher aspect ratio can be achieved when the beam is broadened and a plateau forms. To achieve high-aspect-ratio conditions for the simulations we chose the incident envelope of A_1 to have the shape of a hyper-Gaussian beam of order n with the envelope of A_2 obeying the mirror boundary condition:

$$A_1(x, 0, t) = A_1\exp(-x^{2n}), \tag{10a}$$

$$A_2(x, L, t) = -\sqrt{R}(\mathrm{FT})^{-1}\{\exp(i\phi)\mathrm{FT}[A_1(x, L, t)]\}. \tag{10b}$$

In performing the analytical treatment we have assumed that the homogeneous fixed-point solution is infinitely extended; i.e. we restricted our analysis to an infinitely high aspect ratio. As a consequence, one should expect to encounter discrepancies that become predominant for lower aspect ratios when fewer modulations occur across the unmodulated beam envelope.[19] Here we report the results for $n = 1$ and $n = 4$, which roughly correspond to low and high aspect ratios, respectively, in optical systems. The hyper-Gaussian beam profile ($n = 4$) more closely approximates the assumption of an infinitely extended modulation made in the analysis. We show that the discrepancies remain rather small in this case.

The simulations are done for $f = 0.016$, which corresponds to Fresnel number $F \approx 5$, and for a feedback mirror with reflectivity $R = 1$ placed at the exit face of the crystal ($D = 0$).

A. Constant-Relaxation-Time Approximation

The assumption of constant relaxation time has proved useful in modeling the temporal evolution of spatiotemporal structures in photorefractive wave mixing. Under the approximation of constant relaxation time $\tau(I) = \tau_{\mathrm{PR}}$, the linearized problem, including temporal variation, can be solved analytically, and a threshold equation for the onset of primary instability will be obtained:

$$0 = \cos(\chi_1)\cos(\chi_2) + \left[\frac{\Gamma}{2}\cos(\phi)\cos(\chi_2) + fK^2 \times \left(fK^2 - \frac{\Gamma}{2}\sin(\phi)\right)\mathrm{sinc}(\chi_2)\right] \times \mathrm{sinc}(\chi_1) + \frac{g}{2}\left[\cos(\phi)\cos(\chi_1) + \left(\frac{\Gamma}{2} - fK^2\sin(\phi)\right)\mathrm{sinc}(\chi_1)\right]\mathrm{sinc}(\chi_2), \tag{11}$$

where $\chi_1^2 = (fK^2)^2 - \Gamma^2/4$ and $\chi_2^2(\lambda) = (fK^2)^2 - g^2/4$. Equation (11) reduces to Eq. (5) of Ref. 20 in the case of a stationary instability ($\lambda_c \equiv i\,\mathrm{Im}\,\lambda_c = 0$). The temporal variations in Q that are due to the sluggish PR response result in the function

$$g(\lambda) = \Gamma\frac{\lambda\tau_{\mathrm{PR}}}{\lambda\tau_{\mathrm{PR}} + 1}. \tag{12}$$

The uniform plane-wave solution for the beams loses stability through a saddle-node bifurcation at threshold coupling constant $\Gamma_c L \approx 3.819$. The threshold behavior at the primary instability for the model with $\tau(I) =$ constant is displayed in Fig. 2 for growth rate $\sigma = \mathrm{Re}\,\lambda$ and oscillation frequency $\mathrm{Im}\,\lambda$. A small band

about the critical wave vector has zero frequency. A primary instability in the form of stationary modulation $|W|\cos(K_c x + \psi)$ develops across the uniform solution, with the critical transverse wave vector $fK_c^2 \approx 2.592$, and the transverse phase shift ψ relative to the beam center. In general, ψ changes continuously, because of the translational symmetry. However, in our numerical simulations with hyper-Gaussian beam profiles this symmetry is broken, and ψ may assume discrete values. Two branches of the modulation are identified: those with phases $\psi = 0$ and $\psi = \pi$.

The spatial modes from numerical data are localized in the near field and have a finite spot size in the optical far field. Therefore a mode amplitude is taken as the amplitude of the envelope of the corresponding wave packet. The results are presented summarily in the bifurcation diagram of Fig. 3. For mirror distance $D = 0$ the steady-state amplitude of the modulation is calculated to increase supercritically as $|W| = [(\Gamma - \Gamma_c)/g_s]^{1/2}$, with $g_s \approx 15.69$ given by Eq. (9), and the threshold behavior is similar to that of a second-order phase transition.

Both stable branches are shown in the diagram for both n cases. Close to the predicted threshold the homogeneous solution becomes unstable: first the hyper-Gaussian ($n = 4$) and then the ordinary Gaussian ($n = 1$). The reason for this is that the hyper-Gaussian, with its broad nearly constant intensity plateau, more closely resembles the analytical assumption of an infinitely extended homogeneous state. At the primary instability threshold a stable modulation develops and grows until the secondary instability threshold is approached. The primary modulation is a stationary wave whose wave vector agrees with the calculated value from the linear stability analysis. The analytical curve is also depicted in Fig. 3. For $n = 4$ the overlap between numerical and analytical data turns out to be rather good, despite the still present difference between the high aspect ratio in the first case and the idealized infinitely high aspect ratio in the latter case. Amplitude W of the critical mode and the overall pattern amplitude, which is a superposition of the critical mode amplitude and amplitudes of higher spatial harmonic modes, must clearly be distinguished. They certainly coincide only close to threshold. However, the amplitude of the critical mode obtained from analysis can still give rather accurate results, even far away from threshold, depending on how significant the role of contributions of higher orders in the expansion is. On the contrary, as one might expect, the results for the simple Gaussian beam profile differ considerably.

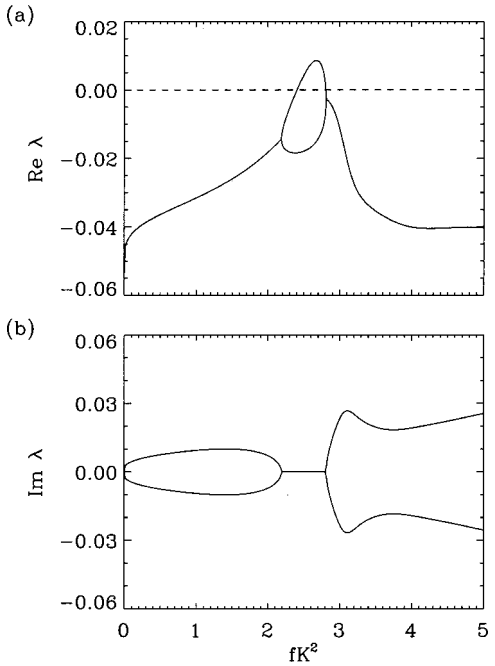

Fig. 2. (a) Growth rates ($\mathrm{Re}\,\lambda$) and (b) oscillation frequencies ($\mathrm{Im}\,\lambda$) of spatial modes K with $\Gamma L = 3.9$ slightly above threshold, for the model with $\tau(I) =$ constant.

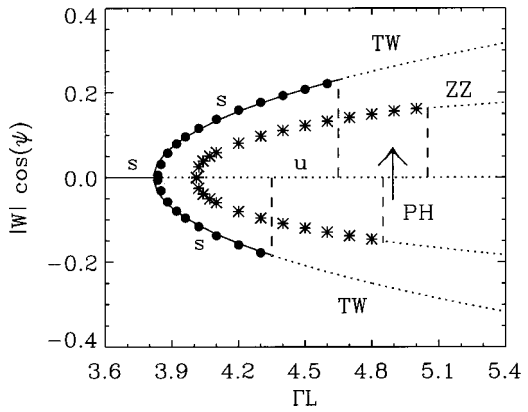

Fig. 3. Bifurcation diagram of the primary and secondary instabilities of beam A_2 at $z = 0$, displaying the amplitude of mode K_c as a function of Γ. Both the hyper-Gaussian (filled circles) and the Gaussian (asterisks) cases are shown, as well as the $\psi = 0$ (upper) and $\psi = \pi$ (lower) branches, obtained from numerical simulations. Solid curves, analytically obtained branches; dotted curves, unstable solutions. Dashed lines mark secondary thresholds for different cases and branches. s's, stable solutions; u, unstable ones. TW's and ZZ are placed where the stable transverse wave and the zigzag, respectively, exist. PH denotes the phase hop, and the arrow designates its direction.

As the secondary instability threshold is approached, different things happen, depending on the specific branch that we are following. Hyper-Gaussian primary modulation invariably loses stability to running transverse waves (TW's), depicted in Fig. 4(a). The threshold for the $\psi = \pi$ branch is lower than the threshold for the $\psi = 0$ branch. The sources and sinks of the TW's are situated on the edges of the modulation-carrying wave. This situation is different from that of counterpropagating two-wave mixing with an external electric field considered earlier,[16,21] in which the secondary source sits in the middle of the wave and radiates TW's left and right toward the sinks at the edges of the wave. The wave vector of a TW remains close to K_c, and its frequency is $\Omega\tau_{\mathrm{PR}} \approx 0.0084$. The nature of secondary bifurcation is a phase instability, and the threshold behavior is similar to that of a first-order phase transition.

The evolution of the secondary instability of the Gaussian carrier wave differs considerably from that of the hyper-Gaussian. The behavior along the two branches changes. The $\psi = \pi$ branch loses stability first; however, it does not develop TW's but jumps over to the $\psi = 0$ stable branch by performing a phase hop, as is pre-

sented in Fig. 5. The sequence of events that leads to the phase-hop instability is shown in Fig. 5(a). Starting from the initial unstable fixed point, the system visits the $\psi = \pi$ branch (repeller). The orbit turns out to be a saddle focus, and this branch, for the given value of Γ, is also unstable. The system then performs a phase hop to reach the stable $\psi = 0$ branch (attractor). We should note that, depending on the perturbation of the initial unstable fixed point, the system may directly revert to the stable attractor without visiting the repeller first.

The secondary instability of the $\psi = 0$ branch of the Gaussian wave [Fig. 4(b)] is not a simple TW. We refer to it as a zigzag instability because of its appearance: The traditional zigzag instability is present in 2D systems only. Apparently, time acts as the second dimension here. Zigzag instability consists of two superposed waves, a running TW and a second wave, with its own wave vector and frequency, riding on it. Hence the secondary instability in this case can be understood as motion on a torus achieved by two Hopf bifurcations from the primary modulation. The two wave vectors and the two frequencies are incommensurate. We did not attempt to drive the structure to spatiotemporal chaos.

B. Intensity-Dependent Relaxation Time

Results presented in Subsection 3.A are valid only under the assumption that the excitation and the recombination of charge carriers that lead to the photorefractive effect have the same time evolution over the entire interaction region. The nonuniform distribution of the total light intensity $I(x,z)$, which is due to pump depletion along the propagation direction and to spatiotemporal modulation in the transverse plane, results in a photorefractive time constant that varies in various regions within the crystal. The PR medium reacts faster in more-illuminated regions, and the buildup of the refractive-index changes proceeds at different paces. As a consequence, the charge transport yields an intensity-dependent photorefractive relaxation time, of the form $\tau(I) = (I_p/I)^{\kappa}\tau_{\mathrm{PR}}$. Nonlinear material response and nonlinear charge diffusion processes in general lead to the values of $\kappa \neq 1$. In particular, numerical investigation of the Kukhtarev band-transport model has been shown to yield a sublinear dependence[11] with $\kappa \approx 0.7$, which is characteristic of inhibited diffusion processes. In the standard Kukhtarev model, assuming a linear medium response, the time constant is calculated to be inversely proportional ($\kappa = 1$) to the total intensity, and Eq. (2) can be written as

$$\tau_{\mathrm{PR}} I_p \partial_t Q + IQ = \Gamma A_1 A_2^* . \tag{13}$$

Owing to this intensity dependence of the temporal evolution, the linear stability of transverse modes depends on the total plane-wave intensity $I^0(z)$ through

$$g(\lambda) = \Gamma \frac{\lambda\tau(I^0)}{\lambda\tau(I^0) + 1}. \tag{14}$$

We solved this nonautonomous stability problem [cf. Eq. (A14)] numerically. The threshold of the primary instability for the model with $\tau(I)$ and $\kappa = 1$ is displayed in Fig. 6. The critical values $\Gamma_c L$ and fK_c^2 remain unaffected because the type of instability is again a saddle-

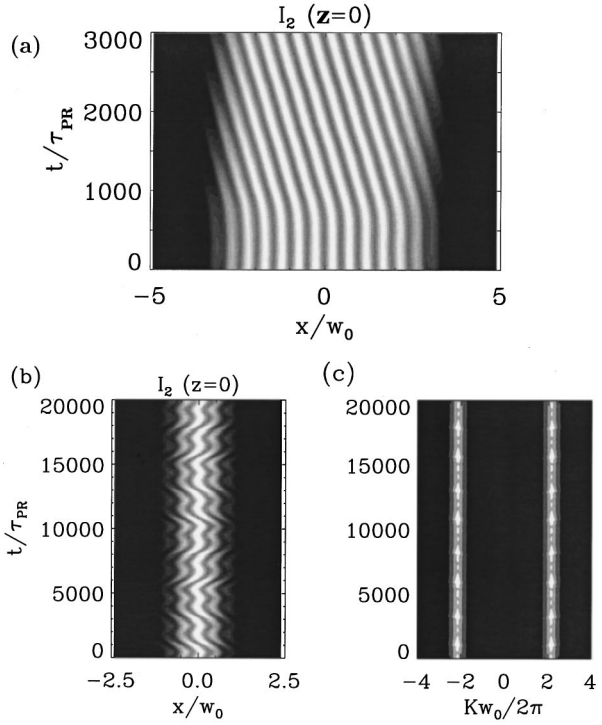

Fig. 4. Transverse intensity profiles of beam A_2 as it leaves the crystal at $z = 0$, above the secondary instability threshold. (a) Developing a running transverse wave in the near field for $n = 4$, $\psi = \pi$, and $\Gamma L = 4.5$. (b) Zigzag instability for $n = 1$, $\psi = 0$, and $\Gamma L = 5.2$. (c) Far-field pattern of (b) with the pump beam subtracted.

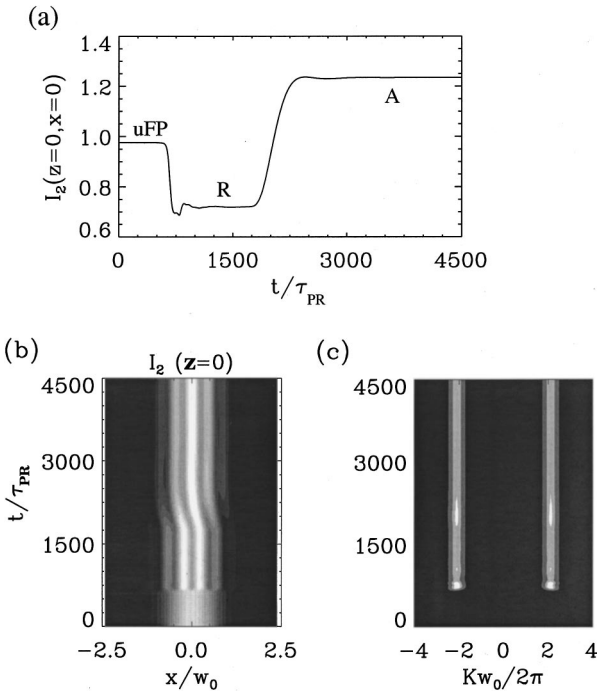

Fig. 5. Intensity of the phase-hop instability at $\Gamma L = 4.9$ for the Gaussian input beam. (a) Intensity of I_2 in the beam center at the exit point as a function of time. uFP, R, and A, unstable fixed point, repeller, and attractor, respectively. (b) Transverse intensity profile I_2 in the near field as a function of time. (c) Far-field pattern of (b) with the pump beam subtracted.

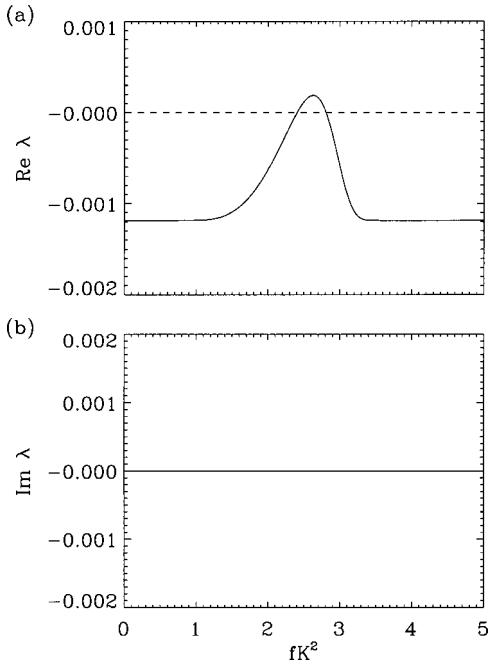

Fig. 6. (a) Growth rates ($\mathrm{Re}\,\lambda$) and (b) oscillation frequencies ($\mathrm{Im}\,\lambda$) of spatial modes K with $\Gamma L = 3.9$, slightly above the primary threshold, for the model with $\tau(I) = \tau_{\mathrm{PR}} I_p / I$.

node bifurcation of the critical mode. All modes turn out to be stationary in this model. The stabilization of the pattern amplitude in Eq. (7) is attained through the same nonlinear coefficient, $g_s \approx 15.69$, independently of κ.

One specific feature that we want to discuss in more detail concerns the linear growth of pattern amplitude, given by the growth rate $\mathrm{Re}\,\lambda$. In contradirectional beam coupling with a feedback mirror and $R = 1$, the total intensity decreases exponentially along the propagation direction $I^0(z) = I^0(0)\exp(-\Gamma z)$. Hence the relaxation time of the crystal $\tau(I^0)$ and, according to Eq. (8), τ_0, increases considerably near $z = L$ and, because of the counterpropagation of beams, slows down the dynamics throughout the crystal. The critical linear growth rate, which is implicitly calculated from the semianalytical threshold condition for this model, is given by

$$\sigma_c(\Gamma) \equiv \mathrm{Re}\left(\frac{\partial \lambda}{\partial \Gamma}\right)_c (\Gamma - \Gamma_c) = \frac{\Gamma - \Gamma_c}{\tau_0} \qquad (15)$$

and can be interpreted in two ways: On one hand, it is the slope of λ when bifurcation parameter Γ passes through the critical value. On the other hand, in view of amplitude equation (7), it provides a time scale for the temporal evolution of a small perturbation of the mode amplitude. We have chosen κ in the interval from 0.0 to 1.0 to be able to compare the approximate model for $\tau(I) = \text{constant}$ ($\kappa = 0$), with the physically more appropriate model, containing the values of κ closer to 1.0. The dynamics of the transverse modulation (Fig. 7) grows on a time scale that is ~2 orders of magnitude larger: $\tau_0(\kappa = 0) \approx 0.45$, whereas $\tau_0(\kappa = 1) \approx 24.9$, with $\tau_0(\kappa)$ given by Eq. (8).

Figure 8 displays the dynamics of relaxation toward a stationary pattern obtained from numerical simulations. Although pattern dynamics is described by a real Landau equation, one finds oscillatory behavior for larger perturbations. For $\kappa = 0$ it relaxes fast, whereas for $\kappa = 1$ the oscillations vanish but the pure relaxation behavior of a small perturbation persists for an exceedingly long period of time [far beyond $10^4 \tau_{\mathrm{PR}}$; Fig. 8(b)], in accordance with the analytical prediction.

Secondary instabilities appear spontaneously for the model with $\kappa = 0$. For $\kappa = 1$ such instabilities have not so far been seen in our numerical simulations. In fact, the secondary patterns for $\kappa = 0$ at high and low aspect ratios are strongly suppressed when they are put into the other model as an initial condition (Fig. 9). This result points to the fact that we must be far away from any possible secondary threshold. For finite Gaussian or hyper-Gaussian beam profiles the time constant at the transverse beam edges, where the temporal evolution is governed by the dark intensity only, is increased even more dramatically. As a consequence, in photorefractive crystals the dynamics is dominated by bright regions, and secondary instabilities, such as running transverse waves

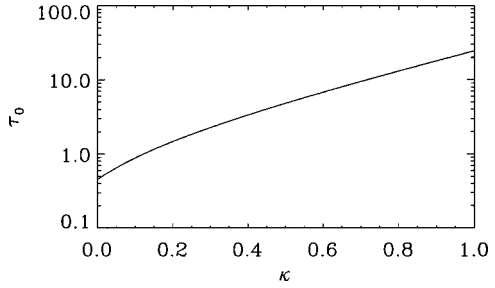

Fig. 7. Logarithmic plot of linear coefficient τ_0 of the amplitude equation for various values of sublinearity parameter κ.

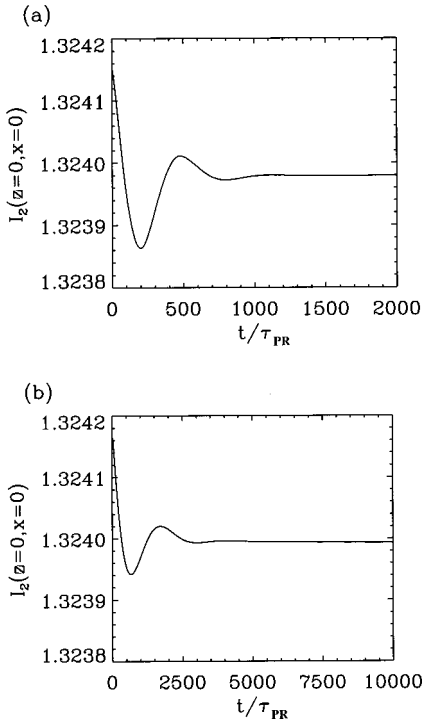

Fig. 8. Transient temporal evolution of the amplitude perturbation for $n = 4$ and $\psi = 0$ at $\Gamma L = 4.6$, for (a) $\kappa = 0$ and (b) $\kappa = 1$.

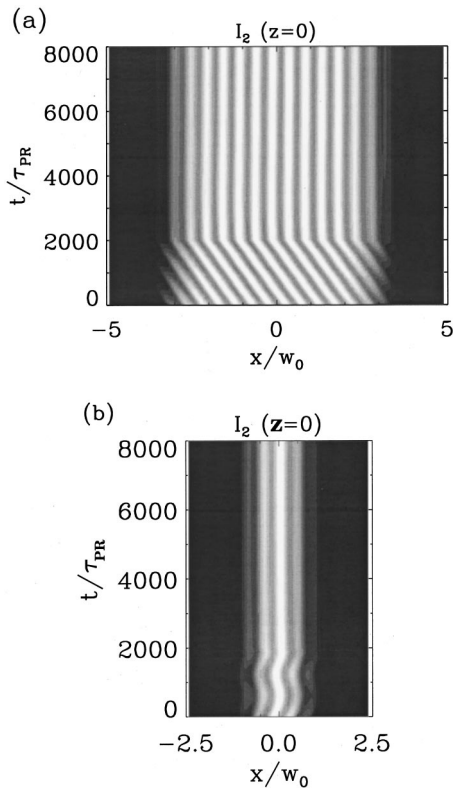

Fig. 9. Spatiotemporal beam profiles displaying a period of $2000\tau_{PR}$ of the secondary attractors [cf. Figs. 4(a) and 4(b)] for the model with $\kappa = 0$, which is then utilized as an initial condition for the model with $\kappa = 1$. (a) Disappearing running transverse wave in the near field for $n = 4$ and $\Gamma L = 4.6$. (b) Disappearing zigzag instability for $n = 1$ and $\Gamma L = 5.2$.

that originate at the beam edges, should have much higher threshold or might even be prevented from appearing.

In addition, one finds that the translational symmetry is recovered and that the stationary modulation of patterns can have arbitrary values of ψ. For the low-aspect-ratio systems this leads to strongly asymmetric transverse profiles [Fig. 9(b)].

4. CONCLUSIONS

We have presented numerical simulations of transverse structures with high and low aspect ratios in a photorefractive feedback system. The amplitude of the critical mode for the high-aspect-ratio beam profile follows the parabolic shape given by the amplitude equation of the Landau-type well, even far above the primary threshold. Allowing for temporal evolution in the linear stability analysis, we have confirmed that for mirror distance $D = 0$ any model with an inhibited diffusion coefficient $\kappa \leqslant 1$ will show stationary patterns, and the common assumption that $\lambda \equiv 0$ is justified here.

We have compared the results for the two models, considering the generic property of the intensity dependence of photorefractive relaxation time. The photorefractive nonlinearity is the same for both models. The intensity dependence has no influence on the steady state or on the shape of transient oscillations, and it does not change our results qualitatively near the primary instability point. In fact, this turns out to be true if the primary instability is of the oscillatory type, for example, when traveling wave patterns occur in the wave-mixing geometry with an externally applied electric field.[21] However, it strongly affects the time scale of the dynamics and the occurrence of secondary patterns. The patterns appear spontaneously in the case of the model with $\kappa = 0$ but seem to have a high threshold for $\kappa = 1$. Whether there is a secondary threshold at all for some value of the coupling strength remains to be seen. Because the oscillation frequency of transverse waves for $\kappa = 0$ is much smaller than the frequency of transient oscillations, we expect this to be true also for any secondary pattern that might appear in the intensity-dependent model. This makes their observation difficult.

APPENDIX A: MULTIPLE SCALE ANALYSIS FOR PHOTOREFRACTIVE WAVE MIXING

In what follows, we present the details involved in using multiple scale analysis to obtain amplitude equation (7) for pattern formation in PR wave mixing.

The general form of wave-mixing equations (6), which we again list here for completeness:

$$\mathcal{L}_{z,x}\mathbf{U} + \mathcal{M}_0\mathbf{P} = \boldsymbol{\mathcal{M}}_1(\mathbf{P}|\mathbf{U}), \tag{A1a}$$

$$(\mathcal{D}_{0,t} + \mathcal{D}_{1,t}(\mathbf{U}) + \mathcal{D}_{2,t}(\mathbf{U}|\mathbf{U}) + \ldots)\mathbf{P} - \mathcal{N}_0\mathbf{U} = \boldsymbol{\mathcal{N}}_1(\mathbf{U}|\mathbf{U}) + \boldsymbol{\mathcal{N}}_2(\mathbf{U}|\mathbf{U}|\mathbf{U}) + \ldots, \tag{A1b}$$

builds the starting point of our expansion procedure, where we follow an idea of Geddes *et al.*[17] for wave mixing in Kerr media that we have modified to be applicable to the grating dynamics that occur in PR wave mixing. These equations are obtained from Eqs. (4) by a basis transformation from complex vectors of deviations to a real $(4 + 2)$-dimensional vector space:

$$\begin{pmatrix} U_1 \\ U_2 \\ U_3 \\ U_4 \end{pmatrix} = \begin{bmatrix} 1 & 1 & -1 & -1 \\ -i & i & -i & i \\ 1 & 1 & 1 & 1 \\ -i & i & i & -i \end{bmatrix} \begin{pmatrix} a_1 \\ a_1^* \\ a_2 \\ a_2^* \end{pmatrix}, \tag{A2a}$$

$$\begin{pmatrix} P_1 \\ P_2 \end{pmatrix} = \begin{pmatrix} 1 & 1 \\ -i & i \end{pmatrix} \begin{pmatrix} q \\ q^* \end{pmatrix}. \tag{A2b}$$

We prefer the $(4 + 2)$-dimensional to the 6-dimensional vector space used by Lushnikov[9] because the grating variables can be eliminated at each order of the expansion, and one is left with a 4-dimensional problem instead.

Equations (A1) are general in the sense that they describe the behavior of wave mixing independently of whether the interactions of field and grating variables originate from two- or four-wave mixing, and they apply to both stationary and oscillatory instabilities.

The notation $(\mathbf{U}|\mathbf{U})$ and $(\mathbf{U}|\mathbf{U}|\mathbf{U})$ denotes products for different quadratic and cubic nonlinearities. For the PR two-wave mixing discussed in the text, the general interaction matrices and vectors are given here for $R = 1$. The spatial and temporal derivative operators are

$$\mathcal{L}_{z,x} = \begin{bmatrix} \partial_z - \Gamma & -f\partial_x^2 & 0 & 0 \\ f\partial_x^2 & \partial_z & 0 & 0 \\ 0 & 0 & \partial_z & -f\partial_x^2 \\ 0 & 0 & f\partial_x^2 & \partial_z - \Gamma \end{bmatrix}, \tag{A3}$$

$$\mathcal{D}_{0,t} = \tau(I^0)\partial_t + 1, \tag{A4}$$

$$\mathcal{D}_{1,t} = -\frac{\kappa}{2}\tau(I^0)U_3\partial_t, \tag{A5}$$

$$\mathcal{D}_{2,t} = -\frac{\kappa}{16}\tau(I^0)[U_1^2 + U_2^2 - 3U_3^2 + U_4^2 - 2(\kappa - 1)U_3^2]\partial_t, \tag{A6}$$

where the matrices $\mathcal{D}_{j,t}$ have been reduced to scalar operators because $\tau(I^0)$ is real valued. The linear coupling matrices read as

$$\mathcal{M}_0 = \Gamma\begin{bmatrix} 0 & 0 \\ 0 & 0 \\ 1 & 0 \\ 0 & 1 \end{bmatrix}, \tag{A7}$$

$$\mathcal{N}_0 = \begin{bmatrix} 0 & 0 & 0 & 0 \\ 0 & 0 & 0 & 1 \end{bmatrix}, \tag{A8}$$

and the nonlinear field–field and field–grating coupling results in the vectors

$$\boldsymbol{\mathcal{M}}_1 = \frac{\Gamma}{4}\begin{bmatrix} P_1 & P_2 & 0 & 0 \\ P_2 & -P_1 & 0 & 0 \\ 0 & 0 & -P_1 & -P_2 \\ 0 & 0 & -P_2 & P_1 \end{bmatrix}\begin{pmatrix} U_1 \\ U_2 \\ U_3 \\ U_4 \end{pmatrix}, \tag{A9}$$

$$\boldsymbol{\mathcal{N}}_1 = -\frac{1}{4}\begin{pmatrix} U_1^2 + U_4^2 \\ U_1U_2 + U_3U_4 \end{pmatrix}, \tag{A10}$$

$$\boldsymbol{\mathcal{N}}_2 = \frac{1}{16}\begin{bmatrix} 2U_3(U_1^2 + U_4^2) \\ 2U_1U_2U_3 - U_4(U_1^2 + U_2^2 - U_3^2 + U_4^2) \end{bmatrix}. \tag{A11}$$

The multiple scale analysis is based on the fact that in the neighborhood of a bifurcation point the temporal and spatial evolution are separable into fast and slow scales. PR coupling strength Γ is the bifurcation parameter, and expansion parameter ϵ scales as the distance from the critical point, Γ_c, at which the modulational instability starts growing. Considering spatially homogeneous distribution of modulation to describe the pattern through a Landau-type formalism, one expands the bifurcation parameter, the temporal variable, and the field and grating amplitudes in terms of ϵ:

$$\Gamma = \Gamma_c + \epsilon\Gamma^{(1)} + \epsilon^2\Gamma^{(2)} + \ldots, \tag{A12a}$$

$$t = T_0 + \epsilon T_1 + \epsilon^2 T_2 + \ldots, \tag{A12b}$$

$$\mathbf{U} = \epsilon^{\nu}\mathbf{U}^{(1)} + \epsilon^{2\nu}\mathbf{U}^{(2)} + \epsilon^{3\nu}\mathbf{U}^{(3)} + \ldots, \tag{A12c}$$

$$\mathbf{P} = \epsilon^{\nu}\mathbf{P}^{(1)} + \epsilon^{2\nu}\mathbf{P}^{(2)} + \epsilon^{3\nu}\mathbf{P}^{(3)} + \ldots. \tag{A12d}$$

The $\Gamma^{(j)}$ are yet unknown quantities to be determined by the multiple scale analysis. As a consequence of these expansions the general interaction vectors and operators are expanded: $\boldsymbol{\mathcal{M}}_j = \boldsymbol{\mathcal{M}}_j^c + \epsilon\boldsymbol{\mathcal{M}}_j^{(1)} + \ldots$ and $\mathcal{L}_{z,x} = \mathcal{L}_{z,x}^c + \epsilon\mathcal{L}^{(1)} + \ldots$, where the unknown part of the bifurcation parameter are factored out: $\mathcal{L}^{(1)} = \Gamma^{(1)}\tilde{\mathcal{L}}$, e.g.

For simplicity, one usually chooses the scaling exponent such that $\nu = 1/2$, therefore *a priori* assuming a specific scaling behavior. We have taken $\nu = 1$, which leads to the same amplitude equation and, in addition, provides the correct scaling behavior to correspond to the characteristics of the underlying bifurcation.

Collecting all terms that are linear in ϵ yields the linear instability threshold; the corresponding solution ansatz introduces the order parameter. Higher orders in ϵ describe the nonlinear interaction of spatial modes and result in the amplitude equation for the order parameter.

In the first order of ϵ one recovers the linear problem:

$$\mathcal{L}_{z,x}^c\mathbf{U}^{(1)} + \mathcal{M}_0^c\mathbf{P}^{(1)} = 0, \tag{A13a}$$

$$\mathcal{D}_{0,T_0}\mathbf{P}^{(1)} - \mathcal{N}_0\mathbf{U}^{(1)} = 0. \tag{A13b}$$

At this point we briefly outline the results from linear stability analyses.[7,8,16] The deviations here can be considered small perturbations, and they are expanded in the transverse Fourier ($x \to K$) and in the temporal Laplace ($T_0 = t \to \lambda$) space, yielding an algebraic expression for $\mathbf{P}^{(1)}$. The linearized equations are cast into matrix form:

$$[\mathcal{L}_z(K) + \mathcal{M}_0\mathcal{D}_0(\lambda)^{-1}\mathcal{N}_0]\mathbf{U}^{(1)} \equiv [\partial_z - \mathcal{A}(z;\lambda,K)]\mathbf{U}^{(1)} = 0, \tag{A14}$$

where the superscript c is discarded because Γ is still a free parameter at this stage. The stability matrix reads as

$$\mathcal{A} = \begin{bmatrix} \Gamma & -fK^2 & 0 & 0 \\ fK^2 & 0 & 0 & 0 \\ 0 & 0 & 0 & -fK^2 \\ 0 & 0 & fK^2 & g(\lambda) \end{bmatrix}. \tag{A15}$$

The temporal variations in Q result in the function $g(\lambda)$ given by Eq. (14) for the general case of an intensity-dependent PR relaxation time, where λ is a complex-valued number.

Owing to the intensity-dependent relaxation time in PR wave mixing, Equation (A14) is nonautonomous and can be solved only numerically. However, under the approximation of constant relaxation time, when $g(\lambda)$ is reduced to Eq. (12) such that the stability matrix is constant in z, the formal analytical solution is given by a linear flow matrix $\mathcal{F}(z) = \exp(\mathcal{A}z)$. Taking into account the mirror boundary conditions [Eqs. (5)], one inverts $\mathcal{F}(L)$ into a scattering matrix $\mathcal{S}_F(K)$. The poles of this matrix determine the properties of absolute instability and lead to the threshold condition [Eq. (11)].

After having discussed the linear instability threshold we come back to the multiple scale analysis. To solve Eqs. (A13) we now make a specific ansatz for a stationary stripelike pattern:

$$\mathbf{U}^{(1)} = \mathbf{u}_{K_c}^{(1)}(z)[W\exp(iK_cx) + \text{c.c.}], \tag{A16a}$$

$$\mathbf{P}^{(1)} = \mathbf{p}^{(1)}_{K_c}(z)[W\exp(iK_c x) + \text{c.c.}]. \tag{A16b}$$

At this stage we introduce mode amplitude $W = W(T_1, T_2, \ldots)$, which may still depend on the slower time scales. The propagation of the transverse modulation through the bulk medium is described by a longitudinal eigenfunction, $\mathbf{u}^{(1)}_{K_c}(z)$. It is calculated from the flow matrix of the linear stability problem:

$$\mathbf{u}^{(1)}_{K_c}(z) = \mathcal{F}(z;K_c)\mathbf{u}^{(1)}_{K_c}(0), \tag{A17}$$

where the vector of initial condition $\mathbf{u}^{(1)}_{K_c}(0)$ belongs to the kernel of the (the inverse of the) scattering matrix $\mathcal{S}_F(K_c)$ and where $\mathbf{p}^{(1)}_{K_c}(z) = \mathcal{N}_0\mathbf{u}^{(1)}_{K_c}(z)$.

As soon as we go to higher orders in the expansion, nonlinear mode interaction occurs and spatial harmonics are generated. From the expansion in 2nd order we have

$$\mathcal{L}^c_{z,x}\mathbf{U}^{(2)} + \mathcal{M}^c_0\mathbf{P}^{(2)} = \mathcal{L}^{(1)}\mathbf{U}^{(1)} - \mathcal{M}^{(1)}_0\mathbf{P}^{(1)} + \boldsymbol{\mathcal{M}}^c_1[\mathbf{P}^{(1)}|\mathbf{U}^{(1)}], \tag{A18a}$$

$$\mathcal{D}_{0,T_0}\mathbf{P}^{(2)} - \mathcal{N}_0\mathbf{U}^{(2)} = -\mathcal{D}_{0,T_1}\mathbf{P}^{(1)} - \mathcal{D}_{1,T_0}[\mathbf{U}^{(1)}]\mathbf{P}^{(1)} + \boldsymbol{\mathcal{N}}_1[\mathbf{U}^{(1)}|\mathbf{U}^{(1)}]. \tag{A18b}$$

For a stationary pattern we have $\mathcal{D}_{0,T_0} = 1$, and in Eq. (A18b) we can solve for grating variable $\mathbf{P}^{(2)}$ and eliminate it from Eq. (A18a) in favor of an inhomogeneous ordinary differential equation for field variable $\mathbf{U}^{(2)}$. The inhomogeneous part generates spatial Fourier modes $K = 0, K_c$, and $2K_c$. Consequently, the solution ansatz is of the form

$$\mathbf{U}^{(2)} = \mathbf{u}^{(2)}_{K=0}(z)(|W|^2 + \text{c.c.}) + \mathbf{u}^{(2)}_{K_c}(z)[V\exp(iK_c x) + \text{c.c.}] + \mathbf{u}^{(2)}_{2K_c}(z)[W^2\exp(2iK_c x) + \text{c.c.}], \tag{A19}$$

where $\mathbf{u}^{(2)}_K(z)$ are the longitudinal eigenfunctions in 2nd order. Because the resonant mode is excited, formally a new amplitude V must be introduced. However, nonlinear contributions are not resonant in this order, and the Fredholm alternative still yields an exponentially unstable behavior. To avoid secular terms we must require that $\partial_{T_1}W = 0$, which then puts the unknown $\Gamma^{(1)} = 0$, and we can choose $V = 0$.

Saturation of the linear exponential growth is at first achieved in 3rd order. From the expansion we have

$$\mathcal{L}_{z,x}\mathbf{U}^{(3)} + \mathcal{M}^c_0\mathbf{P}^{(3)} = \mathcal{L}^{(2)}\mathbf{U}^{(1)} - \mathcal{M}^{(2)}_0\mathbf{P}^{(1)} + \boldsymbol{\mathcal{M}}^c_1[\mathbf{P}^{(1)}|\mathbf{U}^{(2)}] + \boldsymbol{\mathcal{M}}^c_1[\mathbf{P}^{(2)}|\mathbf{U}^{(1)}], \tag{A20a}$$

$$\mathcal{D}_{0,T_0}\mathbf{P}^{(3)} - \mathcal{N}_0\mathbf{U}^{(3)} = -\mathcal{D}_{0,T_2}\mathbf{P}^{(1)} - \mathcal{D}_{0,T_1}\mathbf{P}^{(2)} - \mathcal{D}_{1,T_0}[\mathbf{U}^{(1)}]\mathbf{P}^{(2)} - \mathcal{D}_{1,T_0}[\mathbf{U}^{(2)}]\mathbf{P}^{(1)} - \mathcal{D}_{1,T_1}[\mathbf{U}^{(1)}]\mathbf{P}^{(1)} - \mathcal{D}_{2,T_0}[\mathbf{U}^{(1)}|\mathbf{U}^{(1)}]\mathbf{P}^{(1)} + \boldsymbol{\mathcal{N}}_1[\mathbf{U}^{(1)}|\mathbf{U}^{(2)}] + \boldsymbol{\mathcal{N}}_1[\mathbf{U}^{(2)}|\mathbf{U}^{(1)}] + \boldsymbol{\mathcal{N}}_2[\mathbf{U}^{(1)}|\mathbf{U}^{(1)}|\mathbf{U}^{(1)}]. \tag{A20b}$$

Again, for a stationary pattern, $\mathcal{D}_{0,T_0} = 1$ and $\mathbf{P}^{(3)}$ can be eliminated. Nonlinear mode interaction generates resonant and nonresonant modes. The Fredholm alternative theorem applied to terms that arise from resonant mode K_c determines $\Gamma^{(2)}$. When we return to unscaled units, Eq. (A12a) leads to amplitude equation (7):

$$\tau_0\partial_t W = (\Gamma - \Gamma_c)W - g_s|W|^2 W, \tag{A21}$$

with τ_0 given in Eq. (8). We recognize that up to 3rd order none of the nonlinear temporal derivatives contributes to the dynamics of the Landau equation. Nonlinear self-coupling coefficient g_s, given in Eq. (9), depends on the longitudinal eigenfunctions of 1st and 2nd orders through

$$\mathbf{m}_s = 2\boldsymbol{\mathcal{M}}^c_1[\mathbf{p}^{(1)}_{K_c}|\mathbf{u}^{(2)}_{K=0}] + 2\boldsymbol{\mathcal{M}}^c_1[\mathbf{p}^{(2)}_{K=0}|\mathbf{u}^{(1)}_{K_c}] + \boldsymbol{\mathcal{M}}^c_1[\mathbf{p}^{(1)}_{K_c}|\mathbf{u}^{(2)}_{2K_c}] + \boldsymbol{\mathcal{M}}^c_1[\mathbf{p}^{(2)}_{2K_c}|\mathbf{u}^{(1)}_{K_c}], \tag{A22}$$

$$\mathbf{n}_s = 2\boldsymbol{\mathcal{N}}_1[\mathbf{u}^{(1)}_{K_c}|\mathbf{u}^{(2)}_{K=0}] + 2\boldsymbol{\mathcal{N}}_1[\mathbf{u}^{(2)}_{K=0}|\mathbf{u}^{(1)}_{K_c}] + \boldsymbol{\mathcal{N}}_1[\mathbf{u}^{(1)}_{K_c}|\mathbf{u}^{(2)}_{2K_c}] + \boldsymbol{\mathcal{N}}_1[\mathbf{u}^{(2)}_{2K_c}|\mathbf{u}^{(1)}_{K_c}] + 3\boldsymbol{\mathcal{N}}_2[\mathbf{u}^{(1)}_{K_c}|\mathbf{u}^{(1)}_{K_c}|\mathbf{u}^{(1)}_{K_c}], \tag{A23}$$

where the eigenfunctions of the grating in 2nd order are related to the field eigenfunctions by $\mathbf{p}^{(2)}_K(z) = \mathcal{N}_0\mathbf{u}^{(2)}_K(z) + \boldsymbol{\mathcal{N}}_1[\mathbf{u}^{(1)}_{K_c}(z)|\mathbf{u}^{(1)}_{K_c}(z)]$ for $K = 0$ and $K = 2K_c$.

O. Sandfuchs's e-mail address is oliver.sandfuchs@physik.tu-darmstadt.de.

REFERENCES

1. T. Honda, "Hexagonal pattern formation due to counterpropagation in $KNbO_3$," Opt. Lett. **18**, 598–600 (1993).
2. P. P. Banerjee, H. Yu, D. A. Gregory, N. Kuhktarev, and H. J. Caulfield, "Self-organization of scattering in photorefractive $KNbO_3$ into a reconfigurable hexagonal spot array," Opt. Lett. **20**, 10–12 (1995).
3. C. Denz, M. Schwab, M. Sedlatschek, T. Tschudi, and T. Honda, "Pattern dynamics and competition in a photorefractive feedback system," J. Opt. Soc. Am. B **15**, 2057–2064 (1998).
4. M. Schwab, M. Sedlatschek, B. Thüring, C. Denz, and T. Tschudi, "Origin and control of dynamics of hexagonal patterns in a photorefractive feedback system," Chaos, Solitons Fractals **10**, 701–708 (1999).
5. S. G. Odoulov, M. Y. Goulkov, and O. A. Shinkarenko, "Threshold behavior in formation of optical hexagons and first order optical phase transition," Phys. Rev. Lett. **83**, 3637–3640 (1999).
6. C. Denz, S. J. Jensen, M. Schwab, and T. Tschudi, "Stabilization, manipulation and control of transverse optical patterns in a photorefractive feedback system," J. Opt. B **1**, 114–120 (1999).

7. M. Saffman, A. A. Zozulya, and D. Z. Anderson, "Transverse instability of energy-exchanging counterpropagating waves in photorefractive media," J. Opt. Soc. Am. B **11**, 1409–1417 (1994).
8. T. Honda and P. P. Banerjee, "Threshold for spontaneous pattern formation in reflection-grating-dominated photorefractive media with mirror feedback," Opt. Lett. **21**, 779–781 (1996).
9. P. M. Lushnikov, "Hexagonal optical structures in photorefractive crystals with a feedback mirror," JETP **86**, 614–627 (1998).
10. N. V. Kukhtarev, V. B. Markov, S. G. Odulov, M. S. Soskin, and V. L. Vinetskii, "Holographic storage in electrooptic crystals. I. Steady state," Ferroelectrics **22**, 949–960 (1979).
11. N. Singh, S. P. Nadar, and P. P. Banerjee, "Time-dependent nonlinear photorefractive response to sinusoidal intensity gratings," Opt. Commun. **136**, 487–495 (1997).
12. Z. Zhou, X. Sun, Y. Li, Y. Jiang, H. Zhao, K. Xu, and Q. Wan, "Dynamic solutions of the photorefractive two-wave coupling at large modulation depths," Opt. Commun. **132**, 128–134 (1996).
13. W. Krolikowski, M. R. Belić, M. Cronin-Golomb, and A. Bledowski, "Chaos in photorefractive four-wave mixing with a single grating and a single interaction region," J. Opt. Soc. Am. B **7**, 1204–1209 (1990).
14. M. R. Belić, J. Leonardy, D. Timotijević, and F. Kaiser, "Spatiotemporal effects in double phase conjugation," J. Opt. Soc. Am. B **12**, 1602–1616 (1995).
15. J. Leonardy, F. Kaiser, M. R. Belić, and O. Hess, "Running transverse waves in optical phase conjugation," Phys. Rev. A **53**, 4519–4527 (1996).
16. O. Sandfuchs, F. Kaiser, and M. R. Belić, "Spatiotemporal pattern formation in counterpropagating two-wave mixing with an externally applied field," J. Opt. Soc. Am. B **15**, 2070–2078 (1998).
17. J. B. Geddes, R. A. Indik, J. V. Moloney, and W. J. Firth, "Hexagons and squares in a passive nonlinear optical system," Phys. Rev. A **50**, 3471–3485 (1994).
18. D. Walgraef, *Spatio-Temporal Pattern Formation* (Springer, New York, 1997).
19. G. P. Agrawal, "Transverse modulation instability of copropagating optical beams in nonlinear Kerr media," J. Opt. Soc. Am. B **7**, 1072–1078 (1990).
20. T. Honda and P. P. Banerjee, "Threshold for spontaneous pattern formation in reflection-grating-dominated photorefractive media with mirror feedback," Opt. Lett. **21**, 779–781 (1996).
21. O. Sandfuchs, F. Kaiser, and M. R. Belić, "Influence of dark intensity and intensity-dependent relaxation time on spatiotemporal grating formation," Asian J. Phys. **7**, 629–639 (1998).